VORTEX SHEDDING IN FLOW PAST AN INCLINED FLAT PLATE AT HIGH INCIDENCE

Dan Yang
email: dan.yang@ntnu.no

Helge I. Andersson
email: helge.i.andersson@ntnu.no

Bjørnar Pettersen
email: bjornar.pettersen@ntnu.no

Vagesh D. Narasimhamurthy
email: vagesh.d.narasimhamurthy@ntnu.no

Department of Marine Technology
Norwegian University of Science and
Technology, NO-7491 Trondheim, Norway

Department of Energy and Process Engineering
Norwegian University of Science and
Technology, NO-7491 Trondheim, Norway

ABSTRACT

The properties of asymmetric wake pattern behind a flat plate inclined at angle of attack 20, 25 and 30 degrees are investigated. The Reynolds number based on the plate length is 1000. Both two-dimensional and three-dimensional calculations are performed by direct numerical simulation. The three-dimensional simulation is in better agreement with the experimental data. The asymmetric mean wake flow and coherent patterns in the three-dimensional simulations are also revealed by the time- and phase-averaged techniques and derived the turbulent properties. Unlike the symmetric wake flow, the vortices shed from the leading and trailing edges possess unequal strength. The vortices shed from the trailing edge possess higher strength. The three-dimensional simulation results compare very well with the experimental data.

INTRODUCTION

The flow around bluff bodies has received a great deal of attention over more than a century based on its practical importance in engineering and scientific relevance in fluid mechanics. From the engineering point of view, there are a number of applications in mechanical, civil and naval engineering, such as heat exchangers, bridge piers and offshore platforms. From the fluid mechanics point of view, the flow around bluff bodies involves various important physical phenomena, such as separation, vortex formation, transition to turbulence and vortex induced vibration.

In the flow over a circular cylinder, as the Reynolds number, which base on the free-stream velocity, cylinder diameter, and kinematic viscosity, increases from zero to large values, the wake pattern will experience different kinds of flow regimes. At Reynolds numbers up to approximately 40, the flow is steady laminar flow with a pair of symmetric recirculation bubbles forming behind the cylinder. Then the laminar vortex shedding is observed at Reynolds numbers up to about 190. With a further increase of Reynolds number, two transition regimes called by Williamson (1996) the regime of mode A instability, in the Reynolds number range between 190 and 260, and mode B instability, with Reynolds number of approximately 260, are detected. These two flow regimes have different spanwise wavelength of approximately 4 diameters and 1 diameter respectively. With Reynolds number increases to around 1200 (Prasad and Williamson, 1996, 1997), the shear layers separated from the cylinder become unstable, and for Reynolds numbers beyond 3.5×10^6, the boundary layer on the cylinder becomes turbulent before separation (Kravchenko and Moin, 2000).

The flow around cylinders of other cross-sectional shapes, such as square, flat plates and airfoils, also provide considerable interesting flow mechanisms. Robichaux et al. (1999) performed a Floquet stability analysis of the wake of a square cylinder. The transition scenario appears to be similar to the circular cylinder, with modes A and B instability occurring in the same sequence at the transition Reynolds number of about 160 and 190, respectively. The spanwise wavelengths according to the two modes are 1.2 and 5.5 times the cylinder height (Thompson et al., 2006). Najjar and Balachandar (1998) performed a three-dimensional numerical study of the wake behind a normal flat plate at Reynolds number of 250. They pointed out that the typical low frequency unsteadiness is seen to persist, and affects the flow field as well as the global integral parameters such as the Strouhal number and drag coefficient.

A symmetric wake pattern behind a symmetric bluff body in a uniform flow can be disturbed by the introduction of asymmetric flow conditions. Flow past a rotating circular cylinder is one example (Kang et. al, 1999). As the cylinder rotates, the flow is accelerated on one side of the cylinder and decelerated on the other side. Hence, the pressure on the accelerated side becomes smaller than that on the decelerated side, resulting in a mean lift force. Such a phenomenon is referred to as the Magnus effect. Subsequently, the wake is deflected to one side of the circular cylinder due to the constant rotation and an asymmetric wake pattern was observed.

Linear shear flow past a square cylinder as well as a circular cylinder (Huang et. al., 2010) is another example of asymmetric wake. Discrepancy of mean lift coefficient was reported among investigations both in experiments and numerical simulations. It is attributed to the number of parameters necessary viz., Reynolds number, blockage ratio, three-dimensionality effect, geometry and magnitude of the

shear or combinations of any of these (Lankadasu and Vengadesan, 2010). In the case of nonzero shear, the background vorticity in the free-stream was negative. Therefore, the positive-signed vortices in the near-wake behind the circular cylinder became weakened and elongated, while the negative-signed ones became strengthened and round-shaped (Kang, 2006).

Unlike the rotating circular cylinder and uniform shear flow which lead to the asymmetric wake owing to the unequal velocity on both sides of the cylinder body, the asymmetric wake formed by an inclined flat plate is attributed to the inclination of the plate to the incident free-stream. The early experiment of Fage and Johansen (1927), dealing with a plate at 18 different angles of incidence, showed that the Strouhal number has an approximately constant value of 0.148 at an angle of attack from 30 to 90 degrees.

The vortex shedding occurs from the two edges of an inclined plate, leading to an asymmetric mean velocity field in the very near wake of the recirculation region. It is found that the wake is dominated by a train of counterclockwise vortices shed from the trailing edge of the plate at angle of attack of 30 degrees (Lam, 1996).

The results of the investigation by Perry and Steiner (1987) for angle of attack of 45 degrees revealed that the vortex rolled up from the leading edge was found to remain attached to the rear of the plate for a longer period of time than the trailing edge vortex. The experimental investigation of Lam and Leung (2005) gave detailed velocity fields obtained with particle-image velocimetry (PIV) at successive phases in a vortex shedding cycle at three angles of attack, 20, 25, and 30 degrees, at Reynolds number around 5300. It appeared that the leading edge vortex becomes completely detached from the plate and starts its convection in the wake only at a location near the trailing edge. The measurement region in their experiment was located in the near wake and they didn't give any flow information around the plate

Breuer et al. (2001, 2003) simulated the flow over an inclined plate at 18 degrees, at Reynolds number of 20000 and the computational results showed clearly that the wake is strongly dominated by the trailing edge vortices. It was also reported that there is no regular shedding motion of rotating vortices directly at the leading edge. Instead, behind the leading edge, a Kelvin-Helmholtz instability is detected in the free shear layer. These shear layer vortices develop into a large recirculation region attached to the rear side of the plate.

Zhang et al. (2009) studied the transition route from steady to chaotic state for two-dimensional flows past an inclined flat plate through a systematical study carried out at an attack angle range from 0 to 45 degrees, at Reynolds number less than 800. The results revealed a transition process via the sequential occurrence of the period-doubling bifurcations and the various incommensurate bifurcations.

From the above it is clear that the asymmetric wake conceives different flow characteristics and vortex interactions than the symmetric wake pattern. The two trains of vortices separated alternatively from the leading and trailing edge with opposite rotation and unequal vortex strength. Based on the experiment by Lam and Leung (2005), the different formation mechanisms of the two trains of vortices are believed to result in the different strengths observed between them in the wake. The leading edge vortex had undergone a longer birth history, was more diffused with a lower peak vorticity level at its centre and larger spatial extent of fluid circulation than the trailing edge vortex.

The main objective of the present study is to numerically investigate the formation mechanism of the two trains of vortices, at angle of attack 20, 25 and 30 degrees, as in the experiment of Lam and Leung (2005). The Reynolds number is 1000, based on the plate length. If we adopt the projected length of the plate normal to the incident free-stream as length scale, the Reynolds number for the three different angles of attack are 342, 423 and 500. At these Reynolds numbers, the flow could experience different flow regimes. Details of the flow field around the plate is reported, and the phase-averaged results are exhibited to study the development of individual vortices within a shedding cycle.

NUMERICAL DETAILS

The problem we considered in the present study is flow around an inclined flat plate, as shown in figure 1. The unsteady, incompressible Navier-Stokes equations are solved directly. The non-dimensional form of equations are expressed as

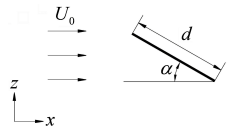

Figure 1. Sketch of free-stream past an inclined flat plate of length d at an angle of attack α.

$$\frac{\partial u_i}{\partial x_i} = 0 \tag{1}$$

$$\frac{\partial u_i}{\partial t} + u_j \frac{\partial u_i}{\partial x_j} = -\frac{\partial p}{\partial x_i} + \frac{1}{\mathrm{Re}} \frac{\partial^2 u_i}{\partial x_j \partial x_j} \tag{2}$$

where the indices $i, j = 1,2,3$ refer to the streamwise (x), spanwise (y), and crossstream (z) directions of the Cartesian coordinate system, respectively. Both two- and three-dimensional numerical simulations are done. The Reynolds and Strouhal numbers are defined as $\mathrm{Re} = U_0 d/\nu$, $\mathrm{Re}' = U_0 d \cdot \sin\alpha/\nu$, $St = fd/U_0$, $St' = fd \cdot \sin\alpha/U_0$, where ν is the kinematic viscosity of the fluid, U_0 is the free-stream velocity, d is the plate length, $d' = d \cdot \sin\alpha$ is the projected length in crossstream direction, f is the shedding frequency.

A finite-volume code (Manhart, 2004) with non-uniform Cartesian grids, on which the variables are arranged staggered, is used. The spatial discretization of the convective and diffusive fluxes is based on second-order central differences. The momentum equations are advanced in time by fractional time stepping using a third-order Runge-Kutta scheme. For the presentation of the flat plate an immersed boundary technique is used. The plate geometry is represented by a triangular

mesh. The immersed boundary technique provides a smooth representation of the body surface by using third-order least squares interpolation for the interface cells (Peller, et al., 2006).

The computational domain is $25d \times 6d \times 15d$ in x, y and z direction. The upstream and downstream domain sizes are $5d$ and $20d$ with respect to the plate centre located at the mid-point of the front face of the plate. The number of grid points is $672 \times 80 \times 474$ with the smallest grid size $0.005d$ around the plate surface. The computed time step is $0.001d/U_0$.

For the two-dimensional calculation the domain size is the same as the three-dimensional case except in the crosswise direction. The crosswise domain size is chosen as $20d$ to capture the vortex pairing dynamics in the wake, which will be shown in the results section.

At the inlet, a uniform free-stream velocity profile ($u = U_0$, $v = w = 0$) is assumed. At the outlet boundary, the Newmann boundary condition ($\partial u_i/\partial x = 0$) is used for all the velocity components. No-slip conditions are prescribed at the body surface. At top and bottom boundaries, we adopt the slip wall condition ($\partial u/\partial z = \partial v/\partial z = \partial p/\partial z = 0$, $w = 0$). In the spanwise direction, a periodic boundary condition is imposed.

RESULTS AND DISCUSSION

Instantaneous Flow Field

In figure 2(a, c, e) temporal variations of the streamwise velocity component for three different angles of attack, measured at downstream point $x = 6.5d$, $y = 2d$, $z = 8d$, which is located behind the plate on the leading edge side, are plotted. The corresponding autocorrelations of the streamwise velocity component are shown in figure 2(b, d, f). Oscillations in the streamwise velocity component for the three-different angles of attack give a clear shedding frequency of the flow (table 1). The periodicity in the autocorrelation figures shows that the flow reaches a relative stable state with almost constant oscillation amplitude for $\alpha = 25^\circ$ and $\alpha = 30^\circ$, figure 2(d, f). It is worth mentioning that in the present simulation, the vortex shedding in the flow around the plate inclined at angle of attack 20 degrees does not maintain a constant shedding frequency in the spanwise direction. There is a small frequency difference along the span, which consequently produces the non-parallel and discontinuous vortex shedding in the wake. More details will be discussed in future work. It is believed that at this angle of attack at the Reynolds number $\mathrm{Re}' = 342$, the flow is undergoing a transition which triggers the low-frequency flow instability in spanwise direction and cause the irregular shedding. It could also be seen from the velocity autocorrelation in figure 2(b), that a low frequency coexists with the main frequency.

The instantaneous contours of spanwise vorticity ω_y are shown in figure 3. Span-averaged values are presented in the cases of three-dimensional computations (figure 3(b, d, f)). The fundamental difference between the two- and three-dimensional simulations is the extended width of the wake. In the cases of three-dimensional simulations the vortex shedding occur alternatively at the leading edge and trailing edge and then form a regular vortex street in the wake. In the cases of two-dimensional simulations (figure 3(a, c, e)), the strong second instability leads to the appearance of the complex aperiodic interaction of the vortices shed from the two edges of the plate and form a wide wake region in the wake. For example at attack angle of 25 degrees (figure 3(c)), a strong aperiodic behavior occurs, while at attack angle of 30 degrees (figure 3(c)), one train of vortex pair is deflected into one side of the wake. The vortex shedding frequencies are compared in table 1. The Strouhal number is lower in the two-dimensional simulation compared to the three-dimensional simulation. The frequency decreases when the angle of attack increases.

Table 1. Comparison of integral quantities defined in terms of the lift (F_L), drag (F_D), and torque (T), $\bar{C}_D = 2F_D/\rho d U_0^2$, $\bar{C}_L = 2F_L/\rho d U_0^2$, $\bar{C}_T = 2T/\rho d U_0^2$, for two-dimensional and three-dimensional simulations at different angles of attack.

α	dimension	$\bar{C}_D$	$\bar{C}_L$	$(-\bar{C}_T)$	St	St'
20	2D	0.3188	1.0381	0.2277	0.4883	0.1670
	3D	0.2880	0.9576	0.2502	0.4959	0.1696
25	2D	0.5827	1.3756	0.2034	0.3967	0.1677
	3D	0.4595	1.1163	0.2697	0.4196	0.1773
30	2D	1.1643	2.1156	0.1528	0.2556	0.1278
	3D	0.6252	1.1902	0.2907	0.3433	0.1717

Time-averaged Flow Field

In figure 4, the mean pressure coefficient, $\bar{C}_p = 2(\bar{p} - p_0)/\rho U_0^2$, based on the time- and span-averaged non-dimensional pressure in three-dimensional simulation at three angle of attack are plotted around the plate surface. Also presented are the two-dimensional simulation results and the experimental data of Fage and Johansen (1927) for angle of attack 30 degrees. The current three-dimensional simulation compares well with the experimental data, whereas the two-dimensional simulation predicts a significantly lower base pressure and fails to capture the flat distribution of pressure on the rear side of the plate as reported in the calculation of Najjar and Balachandar (1998) for a flat plate at angle of attack 90 degrees at $\mathrm{Re} = 250$. This behaivior becomes pronounded as the angle of attack increases, especially near the trailing edge.

The near constant pressure in the base region measured in the experiment is well captured by the three-dimensional simulation. The non-uniform pressure distribution along the base and the higher suction in the two-dimensional simulation make the plate experience higher lift and drag forces, as presented in table 1. At angle of attack 30 degrees, the two-dimensional drag force is 86 % larger than its three-dimensional value and the two-dimensional lift force is 77% larger than in three-dimension. This observation of high drag coefficient predicted in two-dimensionl simulation is in

agreement with what Mittal and Balachandar (1995) concluded in their study on flow over cylinders.

Phase-averaged Flow Field

In order to reduce the background fluctuations and enhance the vortex shedding, the phase-averaged technique is adopted to get the mean values at constant phases. Based on the decomposition scheme of Hussain (1983), the flow velocity signal consists of a time-averaged component $\overline{u}$, a coherent component $\tilde{u}$ and an incoherent random component u', $u = \overline{u} + \tilde{u} + u'$. Ensemble averaging at different phases removes the random component and leaves the phase-averaged velocity $\langle u \rangle$, which contains the mean and coherent component, $\langle u \rangle = \overline{u} + \tilde{u}$. Contours of phase- and span-averaged spanwise vorticity at four sequence phases are depicted in figure 5. It is shown that two trains of vortices with opposite senses of rotation are evident. The trailing edge vortex is formed by roll-up of the shear layer and shed directly from the roll-up location. The shear layers formed at the leading edge extend in streamwise direction over some distance and develop into a big recirculation region. This clockwise vortex remains attached to the plate and is shed into the wake affected by the trailing edge vortex.

From the momentum equation for the mean flow at constant phase, the conventional Reynolds stresses $\langle u_i' u_j' \rangle$, are important from the point of view of coherent structure and generated by spatially local random fluctuations at constant phase. Of equal importance from the point of view of conventional turbulence modeling is $\tilde{u}_i \tilde{u}_j$, which is needed along with $\langle u_i' u_j' \rangle$ for any inquiry into the relative contributions of the periodic and random motions to Reynolds-stress terms in the global mean-momentum equation (Cantwell and Coles, 1983).

Figures 6(a, c, e) show the three Reynolds stresses $\tilde{u}\tilde{u}$, $\tilde{w}\tilde{w}$, $\tilde{u}\tilde{w}$ at phase (3) (figure 5(c)) for the periodic motion. In figure 6(a), with respect to the global mean, the vortex phase motion is essentially a local rotation. This rotation generates peaks in $\tilde{u}\tilde{u}$ contours above and below each vortex, with $\tilde{u}$ positive for one peak and negative for the other. The peaks strength is evidently unequal, for example the peaks above and below the first counterclockwise vortex are 0.3317 and 0.1130. Similarly, the alternative peaks in $\tilde{w}\tilde{w}$ corresponding to the positive and negative peaks in $\tilde{w}$ are shown in figure 6(c), the peaks at x/d =6.4, 7.2, 8.3, 9.4 are 0.4606, 0.2598, 0.1897 and 0.1438 respectively. Figure 6(e) shows the two contributions to the Reynolds shearing stress $\tilde{u}\tilde{w}$. Associated with the periodic motion, the stress doesn't exhibit total antisymmetry, because of the unequal vortex strength. Figures 6(b, c) show the random streamwise and crossstream fluctuations $\langle u'u' \rangle$ and $\langle w'w' \rangle$ at phase (3). The figures show consistently series of peaks for $\langle u'u' \rangle$ and $\langle w'w' \rangle$ corresponding to the vortex centres with connecting ridges in between them, except figure 6(d) shows $\langle w'w' \rangle$ behaving somewhat larger amplitude and stronger peaks at the vortex locations. The contribution to the shear stress by the random turbulence $\langle u'w' \rangle$ is shown in figure 6(f). Unlike the normal stresses due to the random turbulence which have a maximum near each vortex centre the shear stresses due to the random turbulence have an extreme value near the saddle between the vortices.

Figure 7 shows the vortex centre locations and the spanwise peak vorticity at the vortex centres as they are convected downstream. At the two attack angles, the vortex trajectory is not symmetric with respect to the centerline which crosses the plate centre. As the attack angle increase to 30 degrees, the vortex convection route inclined to the leading edge side of the wake for both the leading and trailing edge vortices. When going downstream, the vorticity level, normalized by projected length and velocity U_0, as in Lam and Leung (2005), drops with the growth in vortex size as well as diffusion of vorticity by turbulent actions. The magnitudes of the trailing edge vorticity levels are also plotted to compare with the leading edge vortex. It is evident that the trailing edge vortex possesses a consistently higher level of peak vorticity at its centre along streamwise.

CONCLUSIONS

Two- and three-dimensional numerical simulations of unsteady, incompressible flow around a flat plate inclined at angle of attack 20, 25 and 30 degrees have been carried out. The Reynolds number based on the plate length is 1000. The results show that the two-dimensional simulation gives extremely wide wakes and low pressure in the base region. The three-dimensional simulation gives more realistic flow in the wake, which exhibits a higher strength possessed by the trailing edge vortices. The vortices convection route is inclined to the leading edge side of the wake for both the leading and trailing edge vortices as the plate's angle of attack increase.

REFERENCES

Breuer, M., and Jovicic, N., 2001, "Separated Flow around a Flat Plate at High Incidence: an LES Investigation", *Journal of Turbulence*, Vol. 2, pp. 1-15.

Breuer, M., Jovicic, N., and Mazaev, K., 2003, "Comparison of DES, RANS and LES for the Separated Flow around a Flat Plate at High Incidence", *International Journal for Numerical Methods in Fluids*, Vol. 41, pp. 357-388.

Cantwell, B., and Coles, D., 1983, "An Experimental Study of Entrainment and Transport in the Turbulent near Wake of a Circular Cylinder", *Journal of Fluid Mechanics*, Vol. 136, pp. 321-374.

Fage, A., and Johansen, F. C., 1927, "On the Flow of Air behind an Inclined Flat Plate of Infinite Span", *Proceedings of the Royal Society of London*, Vol. 116, pp. 170-197.

Huang, Z., Narasimhamurthy, V. D., and Andersson, H. I., 2010, " Oblique and Cellular Vortex Shedding behind a

Circular Cylinder in a Bidirectional Shear Flow", *Physics of Fluids*, Vol. 22, 114105-1.

Hussain, A. K. M. F., 1983, "Coherent Structures-reality and Myth", *Physics of Fluids*, Vol. 26, pp. 2816-2850.

Kang, S., Choi, H., and Lee, S., 1999, "Laminar Flow Past a Rotating Circular Cylinder", *Physics of Fluids*, Vol. 11, pp. 3312-3321.

Kang, S., 2006, "Uniform-shear Flow over a Circular Cylinder at Low Reynolds Numbers", *Journal of Fluids and Structures*, Vol. 22, pp. 541-555.

Kravchenko, A. G., and Moin, P., 2000, "Numerical Studies of Flow over a Circular Cylinder at Re_D=3900", *Physics of Fluids*, Vol. 12, pp. 403-417.

Lam, K. M., 1996, "Phase-locked Eduction of Vortex Shedding in Flow Past an Inclined Flat Plate", *Physics of Fluids*, Vol. 8, pp. 1159-1168.

Lam, K. M., and Leung, M. Y. H., 2005, "Asymmetric Vortex Shedding Flow Past an Inclined Flat Plate at High Incidence", *European Journal of Mechanics B/Fluids*, Vol. 24, pp. 33-48.

Lankadasu, A., and Vengadesan, S., 2010, "Shear Effect on Square Cylinder Wake Transition Characteristics", *International Journal for Numerical Methods in Fluids*, Published online in Wiley Online Library, DOI: 10.1002/fld.2408.

Manhart, M., 2004, "A Zonal Grid Algorithm for DNS of Turbulent Boundary Layers", *Computers and Fluids*, Vol. 33, pp. 435-461.

Mittal, R., and Balachandar, S., 1995, " Effect of Three-dimensionality on the Lift and Drag of Nominally Two-dimensional Cylinders", *Physics of Fluids*, Vol. 7, pp. 1841-1865.

Najjar, F. M., and Balachandar, S., 1998, "Low-frequency Unsteadiness in the Wake of a Normal Flat Plate", *Journal of Fluid Mechanics*, Vol. 370, pp. 101-147.

Peller, N., Duc, A. L., Tremblay, F., and Manhart, M., 2006, "High-order Stable Interpolations for Immersed Boundary Methods", *International Journal for Numerical Methods in Fluids*, Vol. 52, pp. 1175-1193.

Perry, A. E., and Steiner, T. R., 1987, "Large-scale Vortex Structures in Turbulent Wakes behind Bluff Bodies. Part 1. Vortex Formation", *Journal of Fluid Mechanics*, Vol. 174, pp. 233-270.

Prasad, A., and Williamson, C. H. K., 1996, ''The Instability of the Separated Shear Layer from a Bluff Body'', *Physics of Fluids*, Vol. 8, pp. 1347-1349.

Prasad, A., and Williamson, C. H. K., 1997, ''The Instability of the Shear Layer Separating from a Bluff Body'', *Journal of Fluid Mechanics*, Vol. 333, pp. 375-402.

Robichaux, J., Balachandar, S., and Vanka, S. P., 1999, "Three-dimensional Floquet Instability of the Wake of Square Cylinder", *Physics of Fluids*, Vol. 11, pp. 560-578.

Thompson, M. C., Hourigan, K., Ryan, K., and Sheard, G. J., 2006, "Wake Transition of Two Dimensional Cylinders and Axisymmetric Bluff Bodies", *Journal of Fluids and Structures*, Vol. 22, pp. 793-806.

Williamson, C. H. K., 1996, "Vortex Dynamics in the Cylinder Wake", *Annual Review of Fluid Mechanics*, Vol. 28, pp. 477-526.

Zhang, J., Liu, N.-S., and Lu, X.-Y., 2009, "Route to a Chaotic State in Fluid Flow Past an Inclined Flat Plate", *Physical Review E*, Vol. 79, pp. 045306: 1-4.

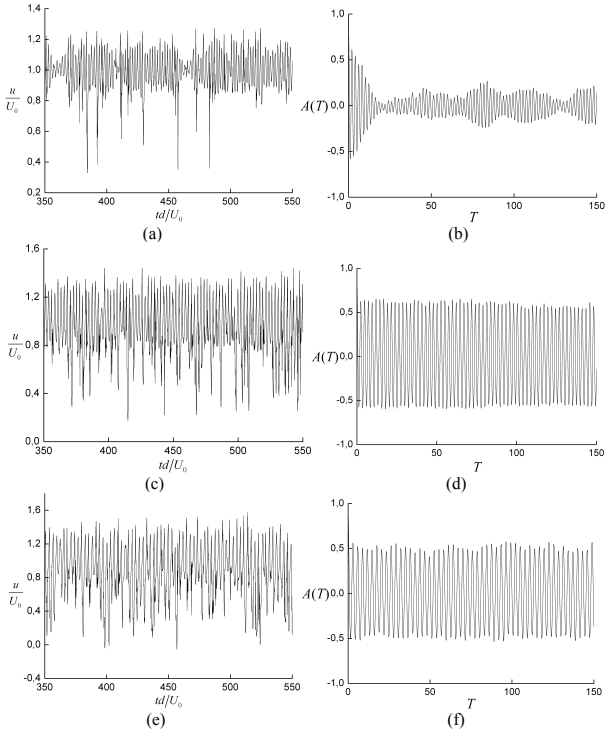

Figure 2. Time signals of the streamwise velocity component at three angles of attack, (a) $\alpha = 20^{\circ}$, (c) $\alpha = 25^{\circ}$, (e) $\alpha = 30^{\circ}$. Corresponding autocorrelations $A(T)$ of the velocity signals are shown in (b, d, f).

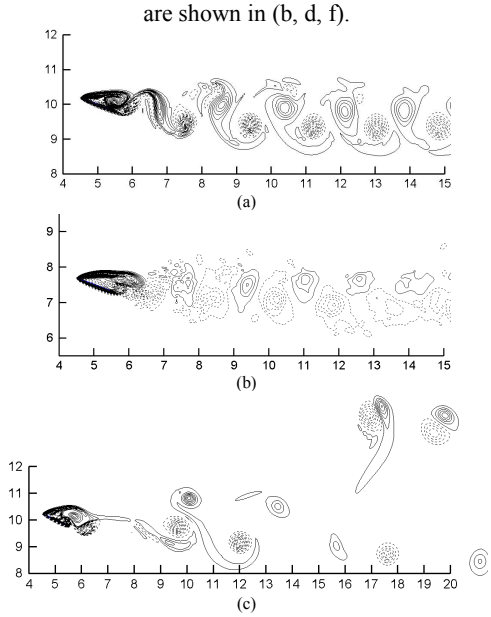

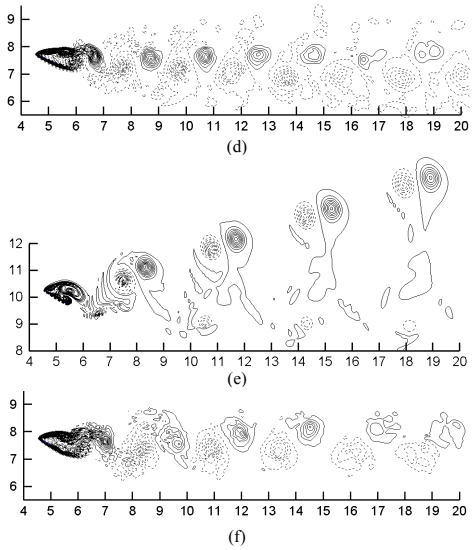

Figure 3. Contour plots of instantaneous spanwise vorticity ω_y in the near wake of the inclined flat plate computed from two-dimensional simulation (a, c, e), three-dimensional simulation (b, d, f), at attack angle of (a, b) $\alpha = 20^\circ$, (c, d) $\alpha = 25^\circ$, (e, f) $\alpha = 30^\circ$. The three-dimensional vorticity field is obtained through span-averaging. Solid (dashed) contours represent clockwise (counterclockwise) rotation. The horizontal and the vertical axis represent the streamwise and the crossstream direction.

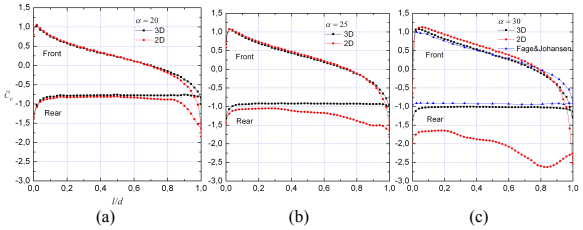

Figure 4. Distribution of the mean pressure coefficient $\overline{C}_P$ along the plate surface obtained from the two- and three-dimensional calculations compared against the experiment ($\alpha = 30^\circ$). Angle of attack (a) 20 degrees, (b) 25 degrees, (c) 30 degrees.

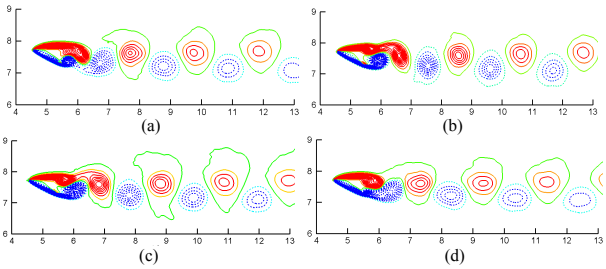

Figure 5. Phase-averaged spanwise vorticity contour at angle of attack 25 degrees, figures (a-d) show the continuous phase in the flow. The horizontal and the vertical axis represent the streamwise and the crossstream direction.

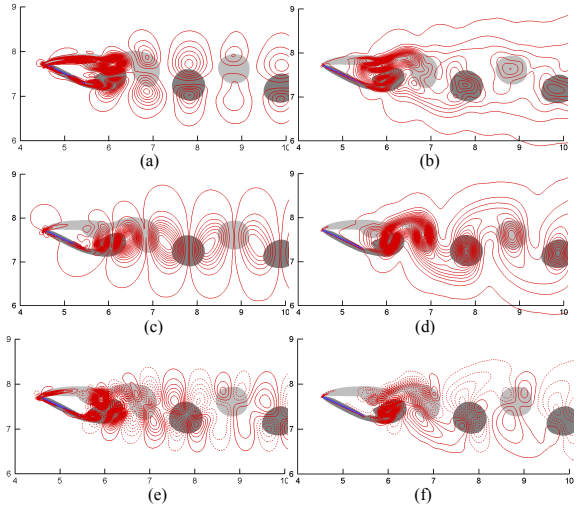

Figure 6. Phase-averaged contours of Reynolds stresses for angle of attack 25 degrees at constant phase (3), (a) $\tilde{u}\tilde{u}/U_0^2$, (b) $\langle u'u' \rangle / U_0^2$, (c) $\tilde{w}\tilde{w}/U_0^2$, (d) $\langle w'w' \rangle / U_0^2$, (e) $\tilde{u}\tilde{w}/U_0^2$, (f) $\langle u'w' \rangle / U_0^2$. Vortices shown by background vorticity regions. Dashed contours for negative values. The horizontal and the vertical axis represent the streamwise x/d and the crosswise z/d direction.

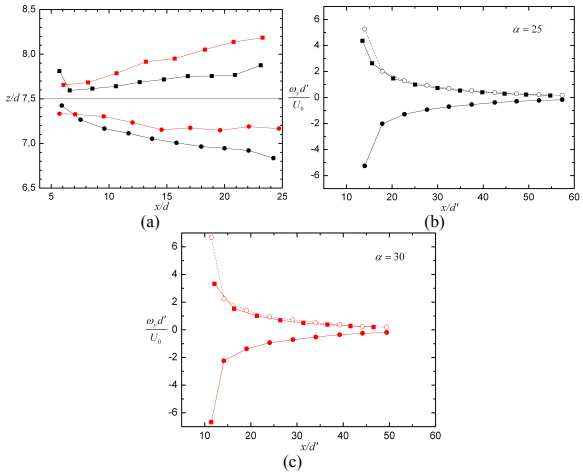

Figure 7. (a) Locations of phase-averaged spanwise vorticity centres. (b)(c) Downstream drop of spanwise peak vorticity levels at vortex centres, positive ω_y for leading edge vortex, negative ω_y for trailing edge vortex, dashed line represent the magnitude of ω_y for the trailing edge vortex. The black and red lines represent the angle of attack 25 and 30 degrees.